Stereographic imaging condition for wave-equation migration[a]

[a]Published in Geophysics, 72 , no. 6, A87-A91, (2007)

Paul Sava (Colorado School of Mines)[1]

ABSTRACT

Imaging under the single-scattering approximation consists of two steps: wavefield reconstruction of source and receiver wavefields from simulated and recorded data, respectively, and imaging from the extrapolated wavefields of the locations where reflectors occur. Conventionally, the imaging condition indicates the presence of reflectors when propagation times of reflections in the source and receiver wavefields match. The main drawback of conventional cross-correlation imaging condition is that it ignores the local spatial coherence of reflection events and relies only on their propagation time. This leads to interference between unrelated events that occur at the same time. Sources of cross-talk include seismic events corresponding to different seismic experiments, or different propagation paths, or different types of reflections (primary or multiple) or different wave modes (P or S). An alternative imaging condition operates on the same extrapolated wavefields, but cross-correlation takes place in a higher-dimensional domain where seismic events are separated based on their local space-time slope. Events are matched based on two parameters (time and local slope), thus justifying the name "stereographic" for this imaging condition. Stereographic imaging attenuates wavefield cross-talk and reduces imaging artifacts compared with conventional imaging. Applications of the stereographic imaging condition include simultaneous imaging of multiple seismic experiments, multiple attenuation in the imaging condition, and attenuation of cross-talk between multiple wavefield branches or between multiple wave modes.

INTRODUCTION

Conventional depth migration consists of two steps: wavefield reconstruction of seismic wavefields at all locations in the imaging volume from data recorded on the acquisition surface, and imaging used to extract reflectivity information from wavefields reconstructed from the sources and receivers. Accurate imaging requires accurate implementation of both steps. Recent seismic imaging research places larger emphasis on wavefield extrapolation than on imaging, partly due to the larger computational cost of extrapolation relative to imaging.

[1]**e-mail:** psava@mines.edu

This paper concentrates on the imaging condition assuming that wavefield extrapolation is performed in a sufficiently accurate velocity model. The imaging condition is often implemented as a cross-correlation of source and receiver wavefields extrapolated from the acquisition surface (Claerbout, 1985). The reason for this choice is that conventional cross-correlation imaging is fast and robust, producing good images in complex environments. The alternative deconvolution imaging condition is not discussed in this paper.

Conventional imaging condition operates in a simple way: source and receiver wavefields are probed to determine the locations where they match, i.e. where the traveltime of events forward-propagated from the source and backward-propagated from the receivers are equal. This is usually achieved by extracting the zero-lag of the temporal cross-correlation between the two wavefields computed at every location in the image. However, this imaging condition ignores the structure of the analyzed seismic wavefields, i.e. the imaging condition does not use the local space-time coherence of the reflected wavefields. This characteristic is contrary to conventional analysis of space-time kinematic coherence of seismic data, which is one of the most important attributes employed in their analysis.

The consequence of this deficiency is that different seismic events present in the extrapolated wavefields interfere with one-another leading to artifacts in seismic images. This interference, also known as cross-talk, occurs between unrelated events which should not contribute to the formed image. It is often possible to identify events that occur at the same time, although they describe different propagation paths in the subsurface. As a consequence, such unrelated events appear as real reflections due to the imaging condition and not due to a geological cause.

This paper presents an extension of the conventional imaging condition. This extension is designed to exploit the local space-time coherence of extrapolated wavefields. Different seismic events are matched both function of propagation time and a local coherence attributes, e.g. local slope measured function of position and time. Therefore, events with different propagation paths are differentiated from one-another, although their propagating time to a given point in the subsurface may be identical (Stolk and Symes, 2004). This property can be used to suppress artifacts due to cross-talk and generate cleaner seismic images.

CONVENTIONAL IMAGING CONDITION

Under the single scattering (Born) approximation, seismic migration consists of two components: wavefield reconstruction and imaging.

Wavefield reconstruction forms solutions to the considered (acoustic) wave-equation with recorded data as boundary condition. We can consider many different numeric solutions to the acoustic wave-equation, which are distinguished, for example, by implementation domain (space-time, frequency-wavenumber, etc.) or type of numeric solution (differential, integral, etc.). Irrespective of numeric implementation, we re-

construct two wavefields, one forward-propagated from the source and one backward-propagated from the receiver locations. Those wavefields can be represented as four-dimensional objects function of position in space $\mathbf{x} = (x, y, z)$ and time t

$$u_s = u_s(\mathbf{x}, t) \quad (1)$$
$$u_r = u_r(\mathbf{x}, t) \ , \quad (2)$$

where u_s and u_r denote source and receiver wavefields. For the remainder of this paper, we can assume that the two wavefields have been reconstructed with one of the numerical methods mentioned earlier.

The second migration component is the imaging condition which is designed to extract from the extrapolated wavefields (u_s and u_r) the locations where reflectors occur in the subsurface. The image r can be extracted from the extrapolated wavefields by evaluating the match between the source and receiver wavefields at every location in the subsurface. The wavefield match can be evaluated using an extended imaging condition (Sava and Fomel, 2005, 2006), where image r represents an estimate of the similarity between the source and receiver wavefields in all 4 dimensions, space ($\mathbf{x}$) and time (t):

$$r(\mathbf{x}, \lambda, \tau) = \int u_s(\mathbf{x} - \lambda, t - \tau)\, u_r(\mathbf{x} + \lambda, t + \tau)\, dt \ . \quad (3)$$

The quantities λ and τ represent the spatial and temporal cross-correlation lags between the source and receiver wavefields. The source and receiver wavefields are coincident (i.e. form an image) if the local cross-correlation between the source and receiver wavefields maximizes at zero-lag on all four dimensions. Other extended imaging conditions (Rickett and Sava, 2002; Biondi and Symes, 2004) represent special cases of the extended imaging condition corresponding to horizontal $\lambda = (\lambda_x, \lambda_y, 0)$, or vertical $\lambda = (0, 0, \lambda_z)$ space lags, respectively. The conventional imaging condition Claerbout (1985) is also a special case of the extended imaging condition 3, corresponding to zero cross-correlation lag in space ($\lambda = 0$) and time ($\tau = 0$):

$$r(\mathbf{x}) = \int u_s(\mathbf{x}, t)\, u_r(\mathbf{x}, t)\, dt \ . \quad (4)$$

The four-dimensional cross-correlation 3 maximizes at zero lag if the source and receiver wavefields are correctly reconstructed. If this is not true, either because we are using an approximate extrapolation operator (e.g. one-way extrapolator with limited angular accuracy), or because the velocity used for extrapolation is inaccurate, the four-dimensional cross-correlation does not maximize at zero lag and part of the cross-correlation energy is smeared over space and time lags (λ and τ). Therefore, extended imaging conditions can be used to evaluate imaging accuracy, for example by decomposition of reflectivity function of scattering angle at every image location (Sava and Fomel, 2003; Biondi and Symes, 2004; Sava and Fomel, 2006). Angle-domain images carry information useful for migration velocity analysis (Biondi and Sava, 1999; Sava and Biondi, 2004a,b; Shen et al., 2005), or for amplitude analysis (Sava et al., 2001), or for attenuation of multiples (Sava and Guitton, 2005; Artman et al., 2007)

The conventional imaging condition 4 is the focus of this paper. As discussed above, assuming accurate extrapolation, this imaging condition should produce accurate images at zero cross-correlation lags. However, this conclusion does not always hold true, as illustrated next.

Figures 1a and 1b represent a simple model of constant velocity with a horizontal reflector. Data in this model are simulated from 3 sources triggered simultaneously at coordinates $x = 600, 1000, 1200$ m. Using the standard imaging procedure outlined in the preceding paragraphs, we can reconstruct the source and receiver wavefields, u_s and u_r, and apply the conventional imaging condition equation 4 to obtain the image in Figure 3a. The image shows the horizontal reflector superposed with linear artifacts of comparable strength.

Figures 2a and 2b represent another simple model of spatially variable velocity with a horizontal reflector. Data in this model are simulated from a source located at coordinate $x = 1000$ m. The negative Gaussian velocity anomaly present in the velocity model creates triplications of the source and receiver wavefields. Using the same standard imaging procedure outlined in the preceding paragraphs, we obtain the image in Figure 5a. The image also shows the horizontal reflector superposed with complex artifacts of comparable strength.

In both cases discussed above, the velocity model is perfectly known and the acoustic wave equation is solved with the same finite-difference operator implemented in the space-time domain. Therefore, the artifacts are caused only by properties of the conventional imaging condition used to produce the migrated image and not by inaccuracies of wavefield extrapolation or of the velocity model.

The cause of artifacts is cross-talk between events present in the source and receiver wavefields, which are not supposed to match. For example, cross-talk can occur between wavefields corresponding to multiple sources, as illustrated in the example shown in Figures 1a-1b, multiple branches of a wavefield corresponding to one source, as illustrate in the example shown in Figures 2a-2b, events that correspond to multiple reflections in the subsurface, or multiple wave modes of an elastic wavefield, for example between PP and PS reflections, etc.

STEREOGRAPHIC IMAGING CONDITION

One possibility to remove the artifacts caused by the cross-talk between inconsistent reflection events is to modify the imaging condition to use more than one attribute for matching the source and receiver wavefields. For example, we could use the time and slope to match events in the wavefield, thus distinguishing between unrelated events that occur at the same time (Figure 4).

A simple way of decomposing the source and receiver wavefields function of local slope at every position and time is by local slant-stacks at coordinates $\mathbf{x}$ and t in the four-dimensional source and receiver wavefields. Thus, we can write the total source

and receiver wavefields (u_s and u_r) as a sum of decomposed wavefields (w_S and w_R):

$$u_s(\mathbf{x},t) = \int w_S(\mathbf{x},\mathbf{p},t)\,d\mathbf{p} \quad (5)$$

$$u_r(\mathbf{x},t) = \int w_R(\mathbf{x},\mathbf{p},t)\,d\mathbf{p}\ . \quad (6)$$

Here, the three-dimensional vector $\mathbf{p}$ represents the local slope function of position and time. Using the wavefields decomposed function of local slope, w_S and w_R, we can design a stereographic imaging condition which cross-correlates the wavefields in the decomposed domain, followed by summation over the decomposition variable:

$$r(\mathbf{x}) = \int\int w_S(\mathbf{x},\mathbf{p},t)\,w_R(\mathbf{x},\mathbf{p},t)\,d\mathbf{p}dt\ . \quad (7)$$

Correspondence between the slopes p of the decomposed source and receiver wavefields occurs only in planes dipping with the slope of the imaged reflector at every location in space. Therefore, an approximate measure of the expected reflector slope is required for correct comparison of corresponding reflection data in the decomposed wavefields. The choice of the word "stereographic" for this imaging condition is analogous to that made for the velocity estimation method called stereotomography (Billette and Lambare, 1997; Billette et al., 2003) which employs two parameters (time and slope) to constrain traveltime seismic tomography.

For comparison with the stereographic imaging condition 7, the conventional imaging condition can be reformulated using the wavefield notation 5-6 as follows:

$$r(\mathbf{x}) = \int\left[\int w_S(\mathbf{x},\mathbf{p},t)\,d\mathbf{p}\right]\left[\int w_R(\mathbf{x},\mathbf{p},t)\,d\mathbf{p}\right]dt\ . \quad (8)$$

The main difference between imaging conditions 7 and 8 is that in one case we are comparing independent slope components of the wavefields separated from one-another, while in the other case we are comparing a superposition of them, thus not distinguishing between waves propagating in different directions. This situation is analogous to that of reflectivity analysis function of scattering angle at image locations, in contrast with reflectivity analysis function of acquisition offset at the surface. In the first case, waves propagating in different directions are separated from one-another, while in the second case all waves are superposed in the data, thus leading to imaging artifacts (Stolk and Symes, 2004).

Figure 3b shows the image produced by stereographic imaging of the data generated for the model depicted in Figures 1a-1b, and Figure 5b shows the similar image for the model depicted in Figures 2a-2b. Images 3b and 5b use the same source receiver wavefields as images 3a and 5a, respectively. In both cases, the cross-talk artifacts have been eliminated by the stereographic imaging condition.

EXAMPLE

The stereographic imaging condition is illustrated with an example derived from the Sigsbee 2A dataset (Paffenholz et al., 2002). Using the model in Figure 6g, two

shots are simulated by wavefield extrapolation modeling, Figures 6a-6c, and a third shot is synthesized by summing the two shots together, Figure 6e. Migration with conventional imaging condition of the three shots produces the images in Figures 6b-6f. The two shots independently illuminate different parts of the model, Figures 6b-6d, while the third composite shot illuminates both sides of the image, Figure 6f. The image produced by the composite shot is populated with artifacts due to the cross-talk between the wavefields originating at the two shot locations.

Figure 6h shows the image obtained by imaging the composite shot, Figure 6e, using the stereographic imaging condition. The image is free of artifacts and shows reflectors extending over the entire image, as would be expected for illumination from two shots at different locations. In this case, the stereographic imaging condition needs to take into account the local dip of the image. Since we cannot know the reflector dip prior to the application of the imaging condition, we need to loop over a range of possible dip angles and decompose the wavefields locally for all possible slope combinations. Thus, the stereographic imaging procedure matches the dip of wavefield components in local windows around every image point. Assuming that the local geologic dip is known, at least approximately, we could consider looping over a small range of local dips, thus decreasing the cost of the imaging condition. This approach was not used for the examples shown in this paper and remains to be investigated by future research.

DISCUSSION

The imaging procedure described in this paper requires additional steps that add to the computational cost of imaging. Furthermore, there are more parameters that need to be chosen. For example, if we use local slant-stacks for local decomposition, we need to decide how many local slopes we should use, how finely we need to sample the slope parameters, how finely in space should we apply slant-stacking of the source/receiver wavefields, etc. The number of local slopes used for the imaging condition depends on wavefield sampling in space and time in order to avoid aliasing. Those challenges remain to be addressed by future research.

In all examples described in this paper, the local windows have simple rectangular shape. However, more sophisticated window types (e.g. Gaussian) are possible alternatives and might improve the quality and efficiency of the method.

We can consider tuning the stereographic imaging condition for specific applications. In current implementation, only image components with spatial coherence (e.g. reflectors) generate wavefields with spatial coherence. Diffractions, for example, do not fit this description and, thus, are removed from the image by the imaging condition. This can be seen both as a feature or as a drawback depending on the type of imaging target.

CONCLUSIONS

Conventional imaging conditions based on cross-correlation of extrapolated wavefields do not take into account the local spatial coherence of reflection events. Events are matched based on their propagation times, which leads to cross-talk between unrelated events. The stereographic imaging condition introduced in this paper operates on seismic wavefields that are first decomposed function of their local slope in space and time. Events are matched based on two parameters (time and local slope), which separates unrelated events and eliminates cross-talk. Higher imaging accuracy is achieved at the expense of larger computational cost. Applications include simultaneous imaging of different seismic experiments (shots), multiple attenuation in the imaging condition, etc.

ACKNOWLEDGMENT

This work is supported by the sponsors of the Center for Wave Phenomena at Colorado School of Mines.

REFERENCES

Artman, B., G. Alvarez, and K. Matson, 2007, Image-space surface-related multiple prediction: Geophysics, **72**, S113–S122.

Billette, F., S. L. Begat, P. Podvin, and G. Lambare, 2003, Practical aspects and applications of 2D sterotomography: Geophysics, **68**, 1008–1021.

Billette, F., and G. Lambare, 1997, Velocity macro model estimation by stereotomography: 59th Mtg., Eur. Assn. Geosci. Eng., Session:P095.

Biondi, B., and P. Sava, 1999, Wave-equation migration velocity analysis: 69th Annual International Meeting, SEG, Expanded Abstracts, 1723–1726.

Biondi, B., and W. Symes, 2004, Angle-domain common-image gathers for migration velocity analysis by wavefield-continuation imaging: Geophysics, **69**, 1283–1298.

Claerbout, J. F., 1985, Imaging the Earth's Interior: Blackwell Scientific Publications.

Paffenholz, J., B. McLain, J. Zaske, and P. Keliher, 2002, Subsalt multiple attenuation and imaging: Observations from the Sigsbee2B synthetic dataset: 72nd Annual International Meeting, SEG, Soc. of Expl. Geophys., 2122–2125.

Rickett, J., and P. Sava, 2002, Offset and angle-domain common image-point gathers for shot-profile migration: Geophysics, **67**, 883–889.

Sava, P., and B. Biondi, 2004a, Wave-equation migration velocity analysis - I: Theory: Geophysical Prospecting, **52**, 593–606.

———, 2004b, Wave-equation migration velocity analysis - II: Subsalt imaging examples: Geophysical Prospecting, **52**, 607–623.

Sava, P., B. Biondi, and S. Fomel, 2001, Amplitude-preserved common image gathers by wave-equation migration: 71st Annual International Meeting, SEG, Expanded Abstracts, 296–299.

Sava, P., and S. Fomel, 2003, Angle-domain common image gathers by wavefield continuation methods: Geophysics, **68**, 1065–1074.

———, 2005, Coordinate-independent angle-gathers for wave equation migration: 75th Annual International Meeting, SEG, Expanded Abstracts, 2052–2055.

———, 2006, Time-shift imaging condition in seismic migration: Geophysics, **71**, S209–S217.

Sava, P., and A. Guitton, 2005, Multiple attenuation in the image space: Geophysics, **70**, V10–V20.

Shen, P., W. Symes, S. Morton, and H. Calandra, 2005, Differential semblance velocity analysis via shot profile migration: 74th Annual International Meeting, SEG, Expanded Abstracts, 2249–2253.

Stolk, C. C., and W. W. Symes, 2004, Kinematic artifacts in prestack depth migration: Geophysics, **69**, 562–575.

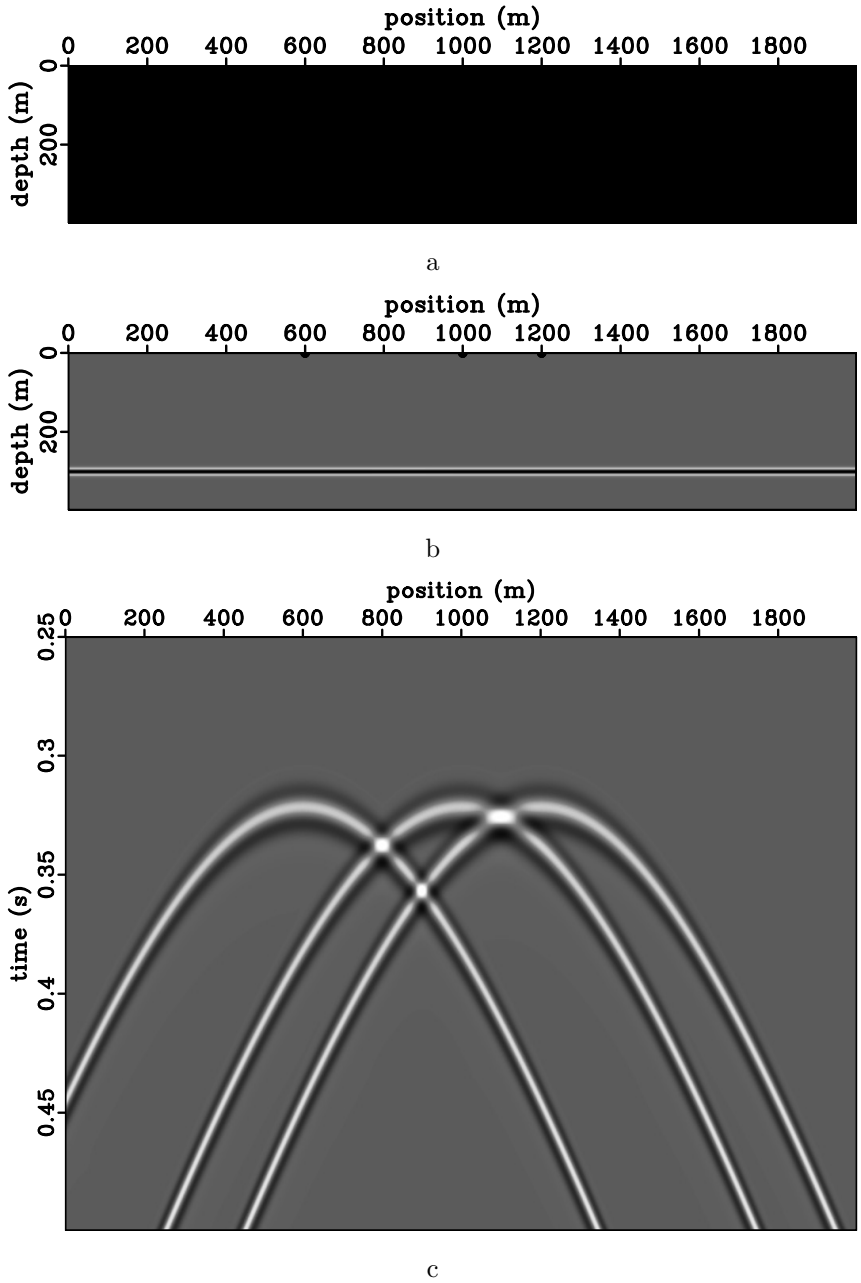

Figure 1: Constant velocity model (a), reflectivity model (b), data (c) and shot locations at $x = 600, 1000, 1200$ m).

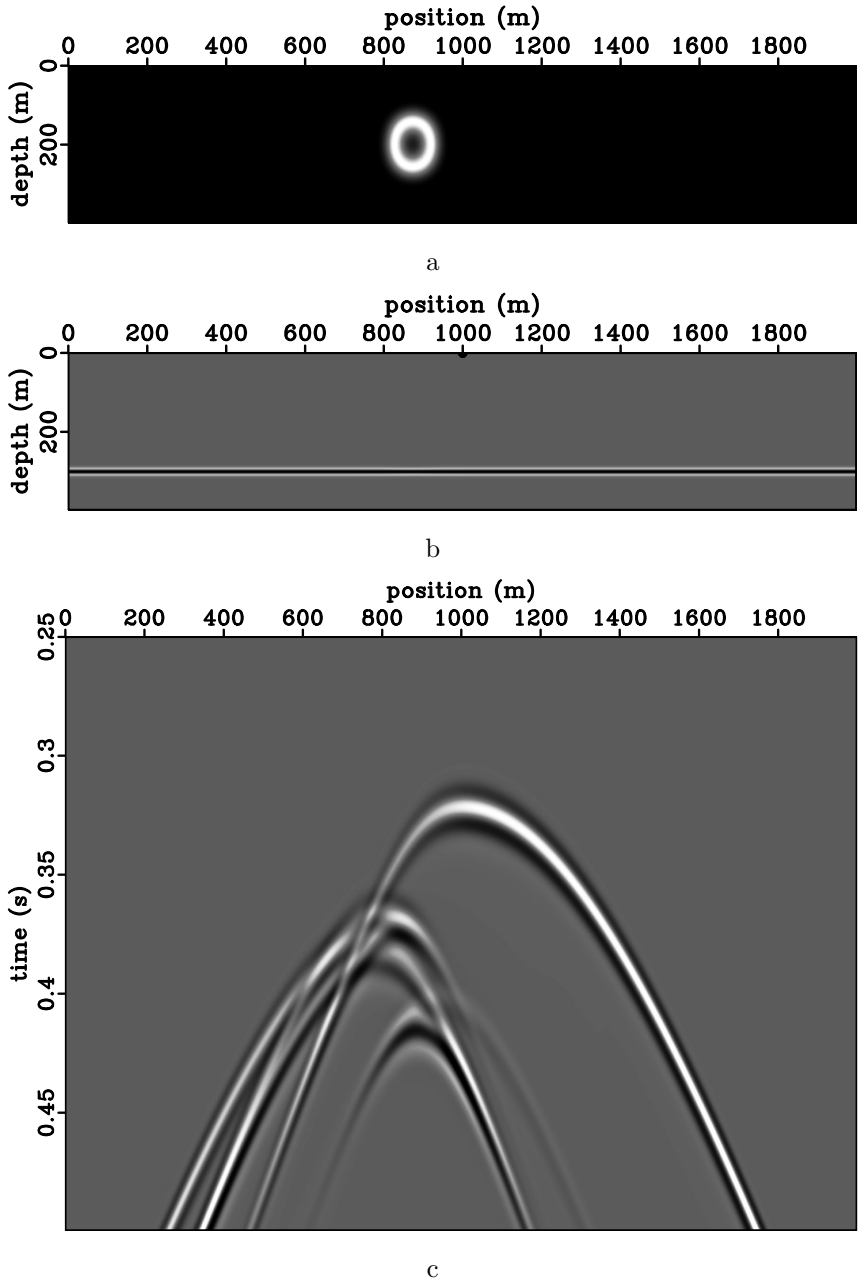

Figure 2: Velocity model with a negative Gaussian anomaly (a), reflectivity model (b), data (c) and shot location at $x = 1000$ m).

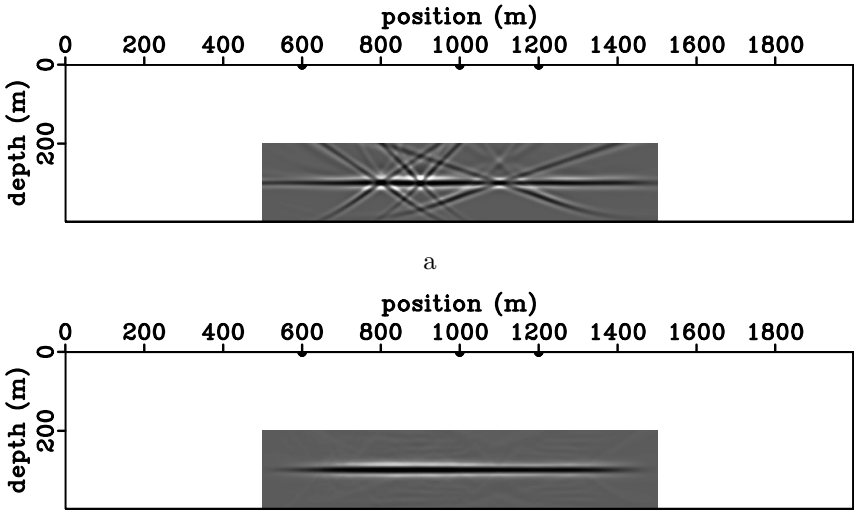

Figure 3: Images obtained for the model in Figures 1a-1c using the conventional imaging condition (a) and the stereographic imaging condition (b).

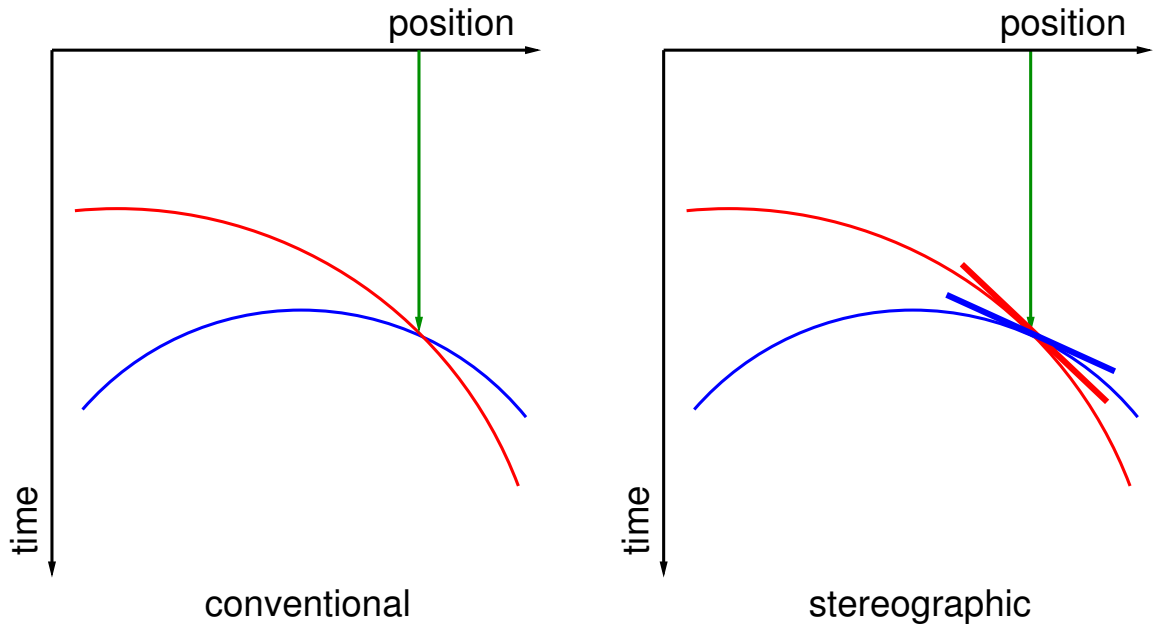

Figure 4: Comparison of conventional imaging (a) and stereographic imaging (b).

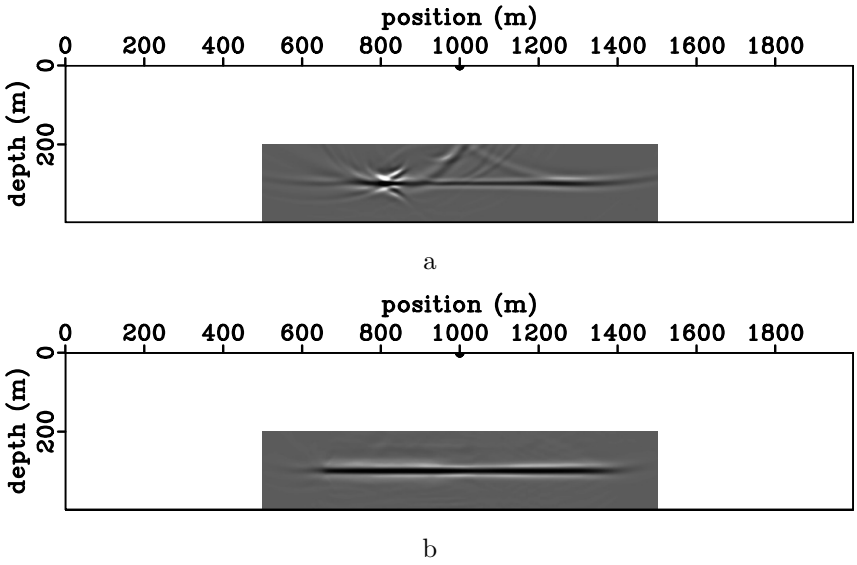

Figure 5: Images obtained for the model in Figures 2a-2c using the conventional imaging condition (a) and the stereographic imaging condition (b).

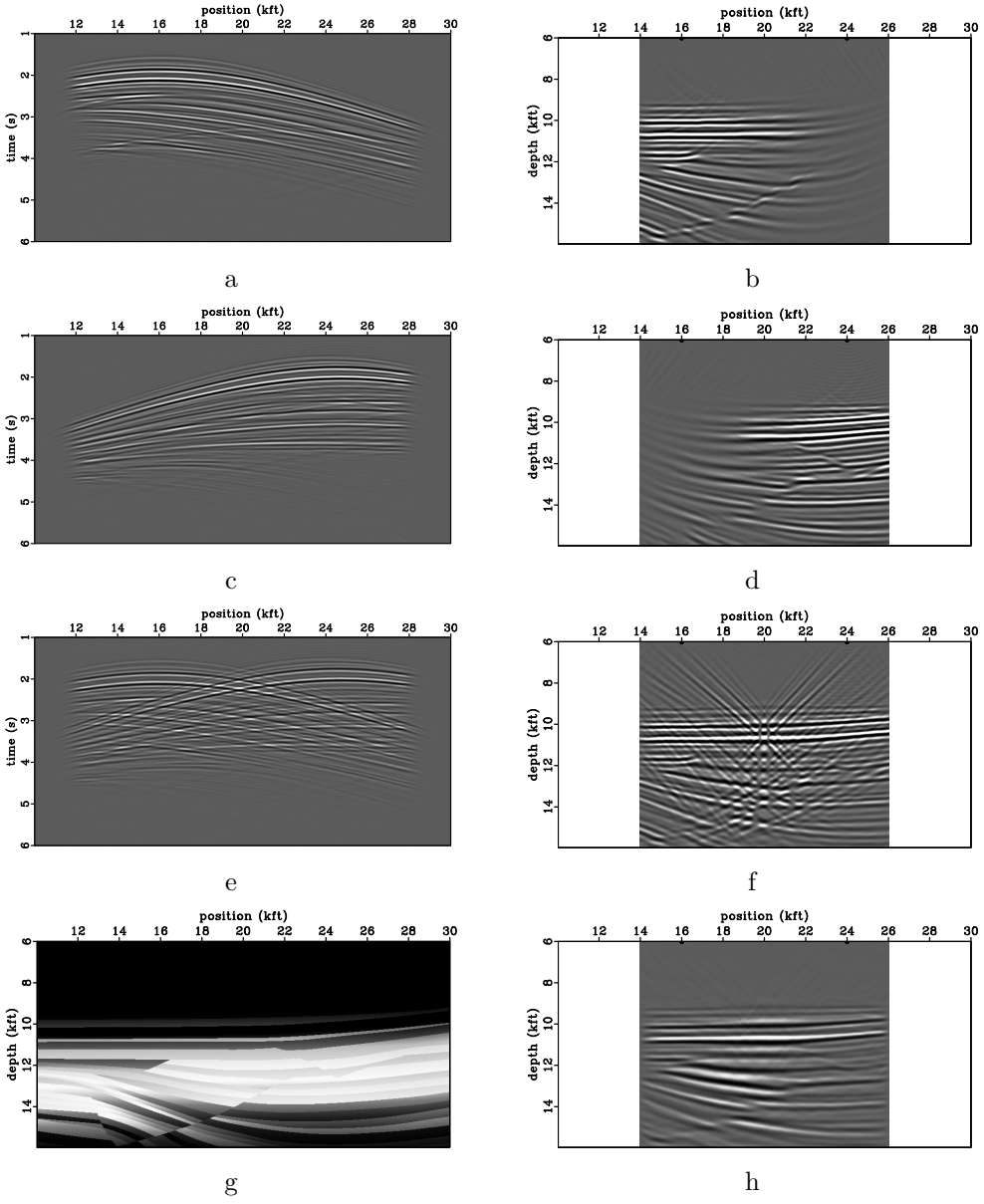

Figure 6: Data corresponding to shots located at coordinates $x = 16$ kft (a), $x = 24$ kft (c), and the sum of data corresponding to both shot locations (e). Image obtained by conventional imaging condition for the shots located at coordinates $x = 16$ kft (b), $x = 24$ kft (d) and the sum of data for both shots (f). Velocity model extracted from the Sigsbee 2A model (g) and image from the sum of the shots located at $x = 16$ kft and $x = 24$ kft obtained using the stereographic imaging condition (h).